Sparsity Promoting Frequency Sampling Method for Estimation of Displacement and Self-Mixing Interferometry Parameters

Junaid Iqbal Khan and Usman Zabit, *Senior Member, IEEE*

***Abstract*—This paper exploits the difference in amplitude spectrum of perturbed and unperturbed phase of self-mixing (SM) laser, to propose a new method for estimation of coupling factor (C), line-width enhancement factor (LEF), as well as displacement of the vibrating target in three major feedback regimes, i.e, weak-, moderate- and strong-feedback regimes. This result thus fills the gap in limitation of previous methods restricted to fewer regimes. The displacement of target is assumed to be bandlimited and sparse in frequency domain. The proposed algorithm showed an average of 1.0168 nm RMS error in displacement estimation corresponding to single- and multi-tone vibrations of amplitudes varying from 3 to 30 times that of laser's wavelength, with percentage error of 1.15% and 3.31% in C and LEF estimations, from simulated SM laser signals. Using an SM sensor based on a laser diode emitting at 785 nm wavelength, the proposed method has achieved an average RMS error of 21 nm in weak-, moderate- and strong-feedback regimes, corresponding to a vibrating target of 5 micrometer peak-peak amplitude.**

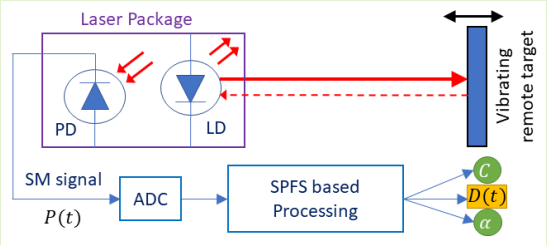

***Index Terms*— Self-mixing, displacement, post-perturbed phase processing, optical feedback coupling factor, linewidth enhancement factor, Fourier transform.**

I. Introduction

SELF-MIXING interferometry (SMI) or optical feedback interferometry has been gaining research attention in the past two decades due to its compactness, cost-effectiveness, and auto-aligned sensing systemic nature [1]–[3]. SMI has found its applications in displacement [4], temperature [5], imaging [6], spectroscopy [7], distance sensing [8], etc.

The signal processing scheme, associated with this setup is simple, i.e, to receive laser power signal, followed by extraction of perturbed phase (with optical feedback), leading ultimately to displacement estimation. But this would be convenient when parameters of SMI are known, i.e, coupling feedback factor (C) and line-width enhancement factor (α). In reality, they are known to be volatile to apparatus's physical conditions. So, complimentary estimation of parameters, alongside with displacement, is a rather robust approach in real time applications.

Manuscript received January 22, 2021; accepted February 9, 2021. Date of publication February 22, 2021; date of current version April 5, 2021. The associate editor coordinating the review of this article and approving it for publication was Dr. Ing. Emiliano Schena. *(Corresponding author: Usman Zabit.)*

The authors are with the Department of Electrical Engineering, National University of Sciences and Technology (NUST), Islamabad 44000, Pakistan (e-mail: jkhan.bee15seecs@seecs.edu.pk; usman.zabit@seecs.nust.edu.pk).

Digital Object Identifier 10.1109/JSEN.2021.3060740

Basic resolution of half-wavelength ($\frac{\lambda}{2}$) can be easily achieved with an SMI sensor under moderate optical feedback regime by fringe counting [2]. The performance can be improved by techniques like phase-locking [9], fringe duplication [10], [11], non-uniform sampling [12], or phase unwrapping methods [13]–[15]. Addressing to the estimation of displacement, complimented with parameters, the proposed method in this paper fundamentally employs Fourier Analysis. On the other hand, variety of Fourier transform based methods [11], [16]–[19] are already present in SMI based sensing, but they are not resilient to all major feedback regimes, i.e, weak, moderate and strong feedback regimes. This paper transcends from the post-perturbed phase processing part of time-frequency signal processing (TFSP) method [17], where the concept of frequency sampling was applied to extract displacement information. The major restriction was that the method did not cover all major optical feedback regimes, with deviation of mean error in displacement estimation from $8nm$ to $20nm$, while going from weak- to moderate-feedback regime.

Infact, there was objectively nothing wrong with the background phenomenon of the algorithm's exploitation, i.e, perturbed phase's spectrum is composed of unperturbed phase's spectrum alongside with excess spectrum, and this behaviour essentially covers all feedback regimes, but the failure of TFSP to cover all feedback regimes implies incompleteness

of the frequency sampling. Furthermore, the same background phenomenon is based on simulation and experimental data, but there isn't any rigorous treatment of such effect present in literature. So instead of relying on an arbitrary collection of observed simulation and experimental data, the authors proved this effect and is termed as the principle of the proposed algorithm, "Sparsity Promoting Frequency Sampling". The proof being slightly lengthy is presented in 'Appendix' section. This algorithm infact covers all major feedback regimes effectively with significant precision in its estimation of parameters of SMI, as well as displacement.

The paper is organized as follows. Fundamentals of SMI are presented in the next section. Then, the proposed algorithm has been developed in 'Algorithm' section, followed by 'Simulations Results' and 'Experimental Verification' sections. The proof of the principle is provided in 'Appendix' section, as it is long and might deflect the reader from proposed algorithm of this paper.

II. Fundamentals of SMI

Theory of SMI is well-established [1]–[3] and is briefly summarized below. Laser beam is generated in the optical cavity of a laser diode (LD) and a portion of the laser beam is back-scattered from the target and re-enters the active laser cavity. Let $D(t)$ represent the instantaneous distance between the LD driven by a constant injection current and the remote surface. Under optical feedback, the laser wavelength is no longer the constant λ_o but is modified to $\lambda_f(t)$ and varies as $D(t)$ varies. The wavelength fluctuations can be found by solving the well-known excess phase equation [2],

$$x_o(t) = x_f(t) + C\sin(x_f(t) + \tan^{-1}(\alpha)) \tag{1}$$

where x_o and x_f are referred to as unperturbed and perturbed phase, respectively. x_o and x_f can be represented as $x_o(t) = 2\pi\nu_o(t)\tau(t)$ and $x_f(t) = 2\pi\nu_f(t)\tau(t)$, where $\tau(t) = 2D(t)/c$ is the round trip time, with c as speed of light. $\nu_f(t)$ and $\nu_o(t)$ represents optical frequency with and without feedback, respectively. Generally, SM sensing is performed under weak feedback regime ($C < 1$), moderate feedback regime ($1 < C < 4.6$), or strong feedback regime ($C > 4.6$). Under optical feedback, laser output optical power $P(t)$ is given by [2],

$$P(t) = P_o[1 + m\cos(x_f(t))] \tag{2}$$

where P_o is the power emitted by the free running LD and m is the modulation index.

In a typical phase unwrapping method, $P(t)$ is used to recover $x_f(t)$. Then, $x_o(t)$ is retrieved via the excess phase equation by using $x_f(t)$ and estimations of C and α parameters. Finally, displacement $D(t)$ of the target is retrieved by using $D(t) = x_o(t)\frac{\lambda_o}{4\pi}$. In the particular case of TFSP [17], frequency domain filtering of $x_f(t)$ (which consisted in setting to zero all those spectral components of $x_f(t)$ having amplitude less than a specific threshold) directly led to very good estimation of $x_o(t)$. The mathematical analysis presented in this paper proves why such an operation leads to very good displacement sensing performance.

III. Principle of SPFS

For a bandlimited sparse displacement in frequency domain, the corresponding SM based perturbed phase's frequency spectrum can be divided into two zones: critical domain (defined as $[-\omega_b, \omega_b]$, where $\omega_b = 2\pi\nu_b$ and ν_b is the bandwidth frequency of the displacement), and outside of critical domain, i.e, $\mathbb{R}/[-\omega_b, \omega_b]$. The amplitude spectrum of perturbed phase occupies larger amplitudes in the critical domain, and smaller amplitudes outside the critical domain and this trend extends to all frequencies in $\mathbb{R}/[-\omega_b, \omega_b]$.

IV. Algorithm Design

A. Frequency Sampling (FS)

The proposed algorithm exploits the principle through frequency sampling, followed by sparsity promotion. FS method is the simplest and direct technique of filtering, which is usually employed when the desired frequency response of the output is known. While it is originally assumed that the displacement is sparse in frequency domain, this combination with the fundamental proposition (which imposes that frequency amplitude spectrum of perturbed phase is modified form of spectrum of unperturbed phase, followed by spread of the spectrum to remaining frequency domain with smaller magnitudes), makes FS of perturbed phase, a natural exploitation.

Once the perturbed phase (x_f) is extracted from laser power signal (P) through methods like phase unwrapping [15], [20], we obtain its amplitude spectrum $A(\nu)$ using FFT of x_f, represented as $F(\nu)$. From this amplitude spectrum (suppose whose range is some set R), if one wishes to automatically sample candidate frequencies corresponding to that of displacement (without resorting to manual thresholds), one could employ algebraic functions that could allow transformations $R \to [0, 1) \to [0, \infty)$. This allows polarization of amplitude spectrum, such that relatively large amplitudes get saturated on considerably larger amplitudes while relatively smaller amplitudes gets diminished significantly. This would not only allow the reduction of operations significantly but also would allow thresholding to be rather automatic, without resorting to manual thresholds. For this paper, the saturation function $\Gamma_l(\omega)$, fitting the above profile, is defined as below:

$$\Gamma_l(\nu) = \frac{\mathcal{N}(A(\nu))^l}{1 - \mathcal{N}(A(\nu))^l} \tag{3}$$

and

$$\mathcal{N}(A(\nu)) = \begin{cases} \dfrac{A(\nu)}{\max(A(\nu))} - \epsilon & A(\nu) = \max(A(\nu)) \\ \dfrac{A(\nu)}{\max(A(\nu))} & A(\nu) \neq \max(A(\nu)) \end{cases}$$

where $A(\nu)$ is the amplitude spectrum of perturbed phase and ν is the frequency. ϵ is small margin added, in order to avoid infinities in (5). $l > 0$ is a sensitivity factor that corresponds to rate at which saturation is achieved.

Once (3) is evaluated, one can extract the candidate frequencies as a set ν_*, defined as follows:

$$\nu_* = \{\Gamma_l(\nu) > \sigma(\Gamma_l(\nu))\} \tag{4}$$

here σ represents standard deviation. Using ν_*, we can sample out the desired frequency spectrum from $F(\nu)$ as $\sum_{n=1}^{N} F(\nu)\delta(\nu-\nu_n)$, where $\nu_n \in \nu_*$ and

$$\delta(\nu) = \begin{cases} 1 & \nu = 0 \\ 0 & \nu \neq 0 \end{cases}$$

Once we frequency sample the perturbed phase and take IFFT, the resultant signal $x_a(t)$ can be written as,

$$x_a(t) = \sum_{n=1}^{N} x_{a_n}(t) \tag{5}$$

where $x_{a_n}(t)$ is a sinusoid corresponding to each sampled frequency. Above can be summarized in the following algorithmic form to obtain $x_a(t)$ from $x_f(t)$, where t is sampled at some sampling frequency.

B. Sparsity Promotion (SP)

1) Successive Displacements: The unperturbed phase x_o is bounded to lie on same frequencies as the sampled frequencies, i.e $\{\nu_n\}_{n=1}^{N}$, as per the principle of the algorithm. Therefore, the relation between x_a and x_o is a combination of translation and scaling. This is because each x_{an} from (8) is a sinusoid, representable as $A_n \sin(2\pi\nu_n t + \theta_n)$, and thus for same ν_n, A_n and θ_n needs to be calibrated to match x_o, and this implies the operations of scaling and translation respectively, in time domain.

We further extrapolate this tuning with successive estimations of parameters C and α, concluded by an objective function. The successive estimation is based on the idea that if we already have some good approximations of parameters, and we algebraically evaluate new values of parameters from (1), by substituting previous values, then the new values would be more accurate. But for that we wish to know some approximation of x_o.

Indeed, x_a acts as good initial approximation of x_o, and it proved to be sufficient representation of x_o for weak feedback regime, as depicted in [17]. Now that x_a is not exactly x_o, but generally close enough, the substitution $x_o \to x_a$ in (1), will make C and α no longer constants, rather function of time as $C'(t)$ and $\alpha'(t)$ respectively, i.e, (1) will be transformed as,

$$\begin{aligned} x_a(t) = x_f(t) &+ C'(t)\cos(\tan^{-1}(\alpha'(t)))\sin(x_f(t)) \\ &+ C'(t)\sin(\tan^{-1}(\alpha'(t)))\cos(x_f(t))) \end{aligned} \tag{6}$$

Proceeding further, in a successive displacement framework, for k^{th} iteration, we algebraically extract either $C'_k(t)$ and $\alpha'_k(t)$ from (6), to be representable as functions of previous iteration $\alpha'_{k-1}(t)$ and $C'_{k-1}(t)$ respectively, alongside with previous estimate of unperturbed phase as $x_{a_{k-1}}(t)$. In this way, we can extract $C'_k(t)$ from (6) as,

$$C'_k(t) = \frac{x_{a_{k-1}}(t) - x_f(t)}{\sin(x_f(t) + \tan^{-1}(\alpha'_{k-1}(t)))} \tag{7}$$

Now from (6), after evaluating $C'_k(t)$, we use it to evaluate $\alpha'_k(t)$. Utilizing $\sin(y) = \sqrt{1-\cos(y)^2}$, solving for $\mu'_k(t) = \sin(\tan^{-1}(\alpha'_k(t)))$ and removing the extraneous solution of the corresponding quadratic equation, we get,

$$\begin{aligned} \mu'_k(t) = \frac{1}{2}&((x_{a_{k-1}}(t) - x_f(t))\cos(x_f(t)) - \sin(x_f(t)) \\ &\sqrt{C'_k(t)^2 - (x_{a_{k-1}}(t) - x_f(t))^2} \end{aligned} \tag{8}$$

So without resorting to $\tan^{-1}(x)$ function, whose approximations are accurate near 0 due to steepness of the function around it, we can extract $\alpha'_k(t)$ as,

$$\alpha'_k(t) = \frac{\mu'_k(t)}{\sqrt{1-\mu'_k(t)^2}} \tag{9}$$

When x_a approaches x_o, then $C'(t)$ and $\alpha'(t)$ from (7) and (9) will become constants C and α of (1), and thus these functions will become equal to their mean and median. As x_a diverges from x_o, $C'(t)$ and $\alpha'(t)$ will homogeneously diverge away from their mean and median. We can take median of these functions as virtual estimates of C and α, which will not only ameliorate computational complexity, but also simplify the dynamics of the algorithm. Median is chosen, as compared to arithmetic mean, as median translates naturally from continuous to discrete domain, while arithmetic mean does not. So, we can replace $\alpha'_{k-1}(t) \to \hat{\alpha}_{k-1}$ and $C'_k(t) \to \hat{C}_k$ in (7) and (8) respectively, where $\hat{\alpha}_{k-1} = median(\alpha'_{k-1}(t))$ and $\hat{C}_k = median(C'_k(t))$.

For each k_{th} iteration, we further attach translation operation (as discussed in the beginning of this section) on $x_{a_{k-1}}(t)$ for evaluation of $\hat{C}_k$ from (7) and scaling operation on $x_{a_{k-1}}(t)$ for evaluation of $\hat{\alpha}_k$.

2) Replacement of Scaling With Offsetting Operation: We can make further improvement by replacing the scaling operation with offsetting, using current estimate $\hat{C}_{k-1}$, as $x_a(t)+\hat{C}_{k-1}-\gamma$, where '$\gamma$' is the offset. This is because (1) can be reduced to following, due to $|sin(x)| \leq 1$ for $x \in \mathbb{R}$ and triangular inequality.

$$|x_o(t)| - |x_f(t)| \leq |x_o(t) - x_f(t)| \leq C \tag{10}$$

$$|x_o(t)| \leq C + |x_f(t)| \tag{11}$$

$$|x_o(t)| = C + |x_f(t)| - \gamma' \tag{12}$$

where $\gamma' \geq 0$ balances the inequality (11) into an equality (12).

Now, since x_a is part of the Fourier spectrum of x_f (with excess frequencies thresholded to zero), therefore, by triangular identity [21],

$$\begin{aligned} |x_a(t)| &= |\int_0^\infty \mathscr{F}\{x_a\}_\omega e^{\iota\omega t} dt| \\ &\leq \int_0^\infty |\mathscr{F}\{x_a\}_\omega| dt \\ &\leq \int_0^\infty |\mathscr{F}\{x_f\}_\omega| dt \geq |x_f(t)| \end{aligned} \tag{13}$$

(13) can be converted to equality, by adding some balancing factor γ'', as $|x_a(t)| + \gamma'' = |x_f(t)|$. In this way, (12) would be reduced to,

$$|x_o(t)| = C + |x_a(t)| - \gamma \tag{14}$$

TABLE I

COMPARISON OF ESTIMATED VALUES OF C AS ($\hat{C}$), α AS ($\hat{\alpha}$) AND CORRESPONDING ROOT-MEAN SQUARE ERROR ($\epsilon_{\hat{D}}$) IN DISPLACEMENT ESTIMATION FOR 6 HZ VIBRATION WITH AMPLITUDE OF 3λ, 30λ VIBRATION CONTAINING 6 HZ AND 12 HZ FREQUENCY COMPONENTS, AND 6λ VIBRATION CONTAINING 6 HZ, 12 HZ, 18 AND 24 HZ COMPONENTS, ACHIEVED ON THREE ITERATIONS (M = 3)

		$3\lambda(6Hz)$			$30\lambda(6Hz)$			$6\lambda(6,12,18,24Hz)$		
C	α	$\hat{C}$	$\hat{\alpha}$	$\epsilon_{\hat{D}}(nm)$	$\hat{C}$	$\hat{\alpha}$	$\epsilon_{\hat{D}}(nm)$	$\hat{C}$	$\hat{\alpha}$	$\epsilon_{\hat{D}}(nm)$
1	9	1.0081	10.1963	0.6833	0.9999	9.3980	0.1517	1.1174	7.5217	3.4410
3	7	3.0163	7.4687	1.4873	2.9966	7.1666	0.4777	3.0021	6.7753	0.6942
5	5	5.0267	4.9619	1.0800	5.0212	4.9831	0.7694	5.0064	4.8935	1.0253
7	4	6.9655	3.9369	1.9056	7.0859	3.9586	3.6132	7.0174	4.0013	0.7235
9	2	8.9800	2.0040	0.8424	8.9198	1.9947	3.5577	8.9477	2.0006	2.2378

where $\gamma = \gamma' - \gamma''$. This replacement has shown to not only ameliorates the convergence of the iterations to desired values, but also decrease the search range by 10-folds. Moreover, removal of scaling operation removes the dependence of iterations on $x_a(t)$, which maybe greatly far from $x_o(t)$, especially in strong feedback regimes.

3) Objective Function: Owing to the assumption that displacement is sparse in frequency domain, i.e, the amplitude spectrum is mostly zero except at a few frequencies, we can attach an objective function that captures this fact. Based on the theory of compressed sensing [22], it is a well established fact that minimal L_1 norm of Fourier transform implies maximal sparsity of Fourier spectrum, thus acting as a substitute to counting the number of non-zero frequency elements. Consequently, we can formulate following objective function using (1), for given x_f, with intermediate estimates of C and α as $\hat{C}_i$ and $\hat{\alpha}_i$, as

$$\begin{aligned}\mathscr{O}(x_f, \hat{C}_i, \hat{\alpha}_i) &= \parallel \mathscr{F}\{\hat{x}_{oi}\} \parallel_1 \\ &= \parallel \mathscr{F}\{x_f + \hat{C}_i \sin(x_f + \tan^{-1}(\hat{\alpha}_i))\} \parallel_1 \quad (15)\end{aligned}$$

4) Smoothing: At the end of k^{th} iteration, when both parameters are estimated, then the k^{th} iteration of unperturbed phase $x_{a_k}(t)$ is estimated using (1). But, even small deviations of estimated parameters, may lead to pulses in $x_{a_k}(t)$, thus inducing high frequency elements into $x_{a_k}(t)$. This can be compensated with application of a smoothing filter. For this paper, a second order Savitzky-Golay filter [23] is employed, which is defined in this paper as $SG_2(x_{a_k}(t), s)$. It is an optimal smoothing filter that tends to fit second order polynomials on subsets of adjacent data points of size 's'.

With above theoretical framework, we can construct Algorithm 2, dealing with sparsity promotion (SP), initialized with some $\hat{\alpha}_0$, maximum M iterations, frame length s of the SG_2 filter, translation range (τ) and offsetting range (η), where τ is an integer, and η is some real number. Moreover, notation is used such that time is shown as discrete function, sampled with some sampling frequency, such that respective intermediate signals are representable under Nyquist-Shannon condition.

C. SPFS Algorithm

By using above mentioned FS and SP algorithms, presented as Algorithm 1 and 2 respectively, we can combine them to form SPFS algorithm, depicted as Algorithm 3, that can estimate parameters C, α, as well as $D(t)$ from given x_f.

Algorithm 1 $x_a(t) = \text{FS}(x_f(t))$

$A(\nu) \xleftarrow{\text{FFT}} x_f(t)$
$\Gamma_l(\nu) \leftarrow A(\nu)$
$\nu_* \leftarrow \Gamma_l(\nu)$
$x_a(t) \xleftarrow{\text{IFFT}} F(\nu) \sum_{n=1}^{N} \delta(\nu - \nu_n)$ ▷ $\nu_n \in \nu_*$

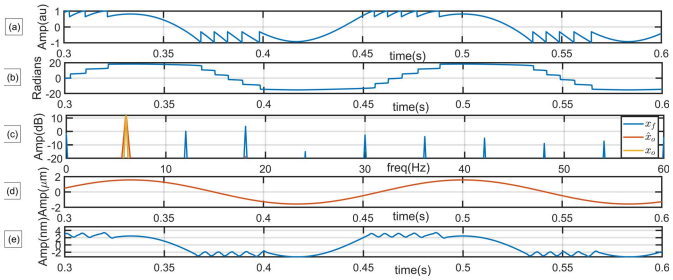

Fig. 1. (a) normalized SM power signal corresponding to target motion with 4λ amplitude containing 6*Hz* frequency component, (b) extracted perturbed phase with reference $C = 10$ and $\alpha = 5$, (c) the absolute of FFT, on dB scale, of simulated x_f, $\hat{x}_o$ and x_o, represented as blue, red and yellow respectively (d) estimated displacement by the proposed algorithm with $\hat{C} = 9.9458$ and $\hat{\alpha} = 4.9928$, and (e) displacement estimation error with respect to reference target motion with RMS value of 2.3818*nm*.

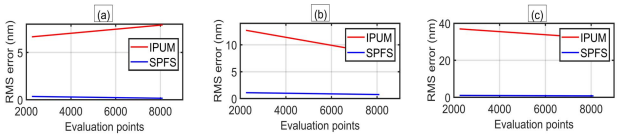

Fig. 2. (a), (b) and (c) represents evolution of the resultant displacement error(nm) in corresponding to number of points searched by the objective function, imparted from IPUM and SPFS, for $C = 1$, $C = 5$ and $C = 10$ respectively.

V. SIMULATION RESULTS

Proposed method has been tested on simulated perturbed phase, extracted from SM signals (in the absence of noise [24], [25] or optical speckle [26]) sampled at $50kHz$, corresponding to 6 Hz vibration with amplitude of 3λ and 30λ, then tested on 6λ vibration having 6 Hz, 12 Hz, 18 Hz and 24 Hz frequency components. Laser's wavelength was set to $\lambda_o = 785\ nm$. The frame length s of Savitzky-Golay filter employed is kept at 301 throughout the simulation and experimental data, and 3 iterations of Algorithm-1 is performed in all simulations.

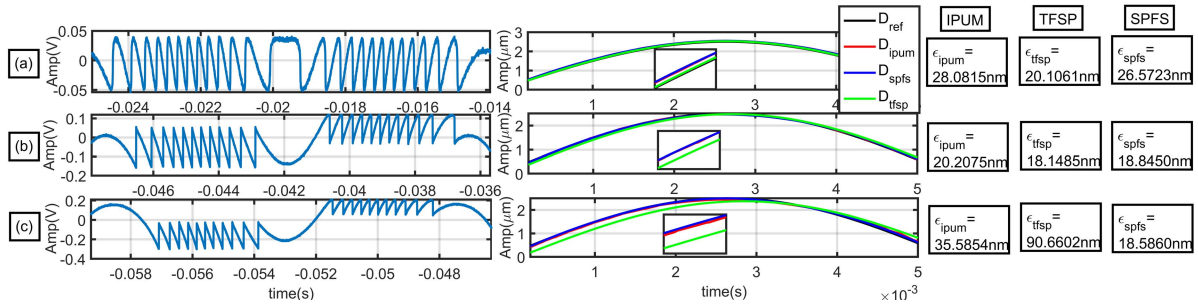

Fig. 3. Plots of experimental SM signals (top to bottom belonging to weak- (a), moderate- (b), and strong- (c) feedback regime respectively) with corresponding retrieved displacement and RMS error, by IPUM, TFSP and proposed SPFS, corresponding to the same remote target PZT motion of $5\mu m$ peak to peak amplitude at $90Hz$, using an SM sensor with HL7851 LD with $\lambda_o = 785nm$.

The results have been documented in Table I for different reference values of 'C' and 'α' over weak-, moderate- and strong-feedback regimes, in the form of estimations as $\hat{C}$ and '$\hat{\alpha}$' with associated RMS error in displacement estimation, represented as '$\epsilon_{\hat{D}}$'.

Algorithm 2 $\{x_{a_M}(t), \hat{C}_M, \hat{\alpha}_M\}$=SP$(x_a(t), \hat{\alpha}_0, M, s, \tau, \eta)$

while $1 \leq k \leq M$ **do**
{
  while $0 \leq m \leq \tau$ **do**
    {
    $x_{a_{k-1}}(t[n+m]) \xleftarrow{\text{translation}} x_{a_{k-1}}(t[n])$
    Evaluate (7) to get $(C'_k(t)$
    $\bar{C}[m] = median(C'_k(t))$
    $O_1[m] = \mathcal{O}(x_f, \bar{C}[m], \hat{\alpha}_{k-1})$
    $m = m + 1$
    {
  m_o=argmin(O_1)
  $\hat{C}_k = C[m_o]$
  $x_{a_{k-1}}(t) = x_{a_{k-1}}(t[n]) = x_{a_{k-1}}(t[n+m_o])$
  $l = 1$
  while $0 \leq \gamma \leq \eta$ **do**
    {
    $x_{a_{k-1}}(t) + \hat{C}_k - \gamma \xleftarrow{\text{offsetting}} \bar{x}_{a_{k-1}}(t)$
    Evaluate (8) to get $\mu'_k(t)$
    $\bar{\mu} = median(\mu'_k(t))$
    $\bar{\alpha_k}[l] = \frac{\bar{\mu}}{\sqrt{1-\bar{\mu}^2}}$
    $O_2[l] = \mathcal{O}(x_f, \hat{C}_k, \bar{\alpha_k}[l])$
    $m = m + 1, l = l + 1$
    $\gamma + \delta\gamma \leftarrow \gamma$
    {
  l_o=argmin(O_2)
  $\hat{\alpha}_k = \bar{\alpha_k}[l_o]$
  $\bar{x}_{a_k}(t) = x_f(t) + \hat{C}_k \sin(x_f + \tan^{-1}(\hat{\alpha}_k))$
  $SG_2(x_{a_k}(t), s) \xleftarrow{\text{smoothing}} \bar{x}_{a_k}(t)$
  $k = k + 1$
}

To show graphical results, the proposed algorithm was applied on perturbed phase extracted from a SM signal corresponding to 7λ, 6 Hz sinusoidal displacement, with reference values $C = 5$ and $\alpha = 5$ (see Fig.1). It can be noted in (c) plot of Fig.1, where a section of absolute FFT, on dB scale, of x_f and x_o are plotted, that the spectrum of x_f covers more amplitudes outside the bandwidth of the displacement, i.e, 6 Hz, thus coherent with the principle of SPFS, and this amplitude invasion extends to whole frequency domain outside 6 Hz.

Algorithm 3 $\{\hat{C}, \hat{\alpha}, \hat{D}(t)\}$=SPFS$(x_f)$

$x_a(t) = FS(x_f)$
$\{x_{a_M}(t), \hat{C}_M, \hat{\alpha}_M\}$=SP$(x_a(t), \hat{\alpha}_0, M, s, \tau, \eta)$
$\hat{D}(t) = \frac{\lambda_o x_{a_M}(t)}{4\pi}$

A. Computational Performance

To analyze the computational performance of SPFS, the objective function (OF) (as represented in (17)) under the construct of SPFS, is compared with that of an established method IPUM [20]. The analysis is performed on simulated perturbed phase signals, corresponding to 3λ displacement, for $C = 1$, $C = 5$ and $C = 10$ respectively, and the number of OF's evaluation points (i.e, the resolution of search domain, where the OF achieves its global minimum) versus the resultant RMS displacement estimation error. The data in plots (a), (b) and (c) of Fig. 2 was acquired by testing the algorithms on a PC 2.8 GHz processor and 8192 MB RAM, and the average CPU run-time of each OF evaluation (total run time of the algorithm divided by the number of evaluations) was 30.6 ms in SPFS case, while 4.4 ms for IPUM. Furthermore, it can be deduced from Fig. 2 for cases $C = 1$, $C = 5$ and $C = 10$, that SPFS's OF is not only numerically stable to change in the size of search domain, but also for same search domain resolution, its resultant estimation error (nm) is considerably less by almost 25 folds, as compared to IPUM, at the cost of increased time complexity by 7 folds.

VI. Experimental Verification

The proposed method is tested by using experimental SMI signals, acquired under different optical feedback conditions but corresponding to the same remote target motion of $5\mu m$ peak to peak amplitude at 90 Hz. The SMI sensor is based on the LD package from Hitachi® (HL7851) emitting laser with a wavelength of 785 nm. The built-in monitor photodiode, placed at the back-facet of LD of HL7851 is used to

access the SMI signals. Optical feedback strength was varied by changing the focus of the lens (having 6.24 mm focal length) mounted inside the collimation tube (model LT110P-B by ThorLabs®) which housed the LD. A commercial PZT (electric Transducer) from Physik Instrumente® is used as the remote target. The PZT is equipped with a built-in capacitive sensor having 2 nm measurement precision.

The proposed method has been compared with IPUM [20] and TFSP [17]. It can be observed that the strong-feedback regime SM signal is affected by one lost fringe [8], as shown in Fig. 3 (c). Thus the proposed method excels IPUM individually in each feedback regime with average precision of 21.3344nm, whilst IPUM's precision is 27.9581nm. On the other hand, TFSP delivered slightly better precision in weak and moderate-feedback regimes, with a dramatic downfall in strong-feedback regime, producing an overall precision of 42.9716nm. The above results show the generality of proposed algorithm with sufficient precision.

VII. Conclusion

In this work, main idea of time domain-frequency domain signal processing (TFSP) [17], which is solely frequency sampling with pre-knowledge of threshold, has been extensively and originally developed into an algorithm, paved by the principle of SPFS. Not only the principle is proved, so that one can easily employ SPFS without running into exceptions, but also the resultant method can efficiently estimate both key parameters of self-mixing interferometry, as well as displacement over the three major optical feedback regimes. The accuracy of C and α estimations, obtained from noiseless simulations for different cases of displacement ranging from 3 to 30λ amplitudes containing single and multiple harmonics for reference values $C = 1$ to 10 and $\alpha = 2$ to 9, obtained was 1.15% and 3.31% respectively, while mean error in displacement estimation obtained was 1.0168nm.

For experimental SM signals with $\lambda_o = 785nm$, affected by noise, the method was tested and compared with methods IPUM and TFSP for weak-, moderate- and strong-feedback regime cases. The precision obtained by proposed method was 21.3344nm as compared to 27.9581nm and 42.9716nm precision of IPUM and TFSP respectively. Reference PZT sensor with 2 nm resolution was used to quantify these experimental displacement sensing performances.

Appendix

Following provides the proof of the principle of SPFS. Without loss of generality, from equation (1), after adding $\tan^{-1}(\alpha)$ on both sides and letting $x'_o = x_o + \tan^{-1}(\alpha)$ and $x'_f = x_f + \tan^{-1}(\alpha)$,

$$x'_o = x'_f + C\sin(x'_f) \tag{16}$$

Defining $\epsilon = x'_f - x'_o$, equation (16) becomes,

$$\epsilon = -C\sin(x'_f) \tag{17}$$

Taking Fourier Transform, represented as $\mathscr{F}[]_\omega = \int_0^\infty [] e^{-\imath\omega t} dt$, on both sides.

$$\mathscr{F}[\epsilon]_\omega = -C\mathscr{F}[\sin(x'_f)]_\omega \tag{18}$$

Expanding $\sin(x'_f)$ as its Taylor series and after employing convolution theorem [21] followed by L_2 norm, we get,

$$\| \mathscr{F}[\epsilon]_\omega \|_2 = C \| \sum_{k\geq 0} (-1)^k \frac{*_1^{2k+1}\mathscr{F}[x'_f]_\omega}{(2k+1)!} \|_2 \tag{19}$$

where $(2k+1)$ times self-convolution is represented as $*_1^{2k+1}$. (19) can be rewritten as,

$$\| \mathscr{F}[\epsilon]_\omega \|_2 = C \| \sum_{k\in even} \frac{*_1^{2k+1}\mathscr{F}[x'_f]_\omega}{(2k+1)!} - \sum_{k\in odd} \frac{*_1^{2k+1}\mathscr{F}[x'_f]_\omega}{(2k+1)!} \|_2 \tag{20}$$

Under frame of triangular inequality [21], for measurable functions 'a' and 'b',

$$\| a \|_2 - \| b \|_2 \leq \| a - b \|_2 \leq \| a \|_2 + \| b \|_2 \tag{21}$$

Moreover, $\| f * f \|_2 \leq \| f \|_1 . \| f \|_1$ [21], which implies,

$$\| *_1^{2k+1} f \|_2 \leq (\| f \|_1)^{2k+1} \tag{22}$$

Using (RHS) inequality of (21) in (20),

$$\| \mathscr{F}[\epsilon]_\omega \|_2 \leq C \sum_{k\geq 0} \frac{(\| \mathscr{F}[x'_f]_\omega \|_1)^{2k+1}}{(2k+1)!} \leq C \sinh \| \mathscr{F}[x'_f]_\omega \|_1 \tag{23}$$

Now from equation (20), applying (LHS) inequality of (21),

$$\| \mathscr{F}[\epsilon]_\omega | \|_2 \geq C \| \sum_{k\in even} \frac{*_1^{2k+1}\mathscr{F}[x'_f]_\omega}{(2k+1)!} \|_2 - C \| \sum_{k\in odd} \frac{*_1^{2k+1}\mathscr{F}[x'_f]_\omega}{(2k+1)!} \|_2 \tag{24}$$

Focusing on the second normed sum on RHS of inequality (24),

$$\begin{aligned} & C \| \sum_{k\in odd} \frac{*_1^{2k+1}\mathscr{F}[x'_f]_\omega}{(2k+1)!} \|_2 \\ & \leq C \sum_{k\in odd} \frac{(\| \mathscr{F}[x'_f]_\omega \|_1)^{2k+1}}{(2k+1)!} \\ & \leq C \sum_{k\geq 0} \frac{(\| \mathscr{F}[x'_f]_\omega \|_1)^{2k+1}}{(2k+1)!} = C.\sinh \| \mathscr{F}[x'_f]_\omega \|_1 \end{aligned} \tag{25}$$

For first normed sum on RHS of inequality (24), letting

$$f(x'_f) = \| \sum_{k\in even} \frac{*_1^{2k+1}\mathscr{F}[x'_f]_\omega}{(2k+1)!} \|_2 \tag{26}$$

By again using triangular inequalities, and by adding and subtracting suitable terms for higher bound (alongside with converting L_2 norm to L_1 norm) and truncating at $k = 0$ for the lower bound, we can find

$$\| \mathscr{F}[x'_f]_\omega \|_2 \leq f(x'_f) \leq \frac{\sin(\| \mathscr{F}[x'_f]_\omega \|_1) + \sinh(\| \mathscr{F}[x'_f]_\omega \|_1)}{2} \tag{27}$$

Replacing second normed sum (which is always positive) in (24) with something bigger will preserve the inequality of (24). Therefore, combining results from inequality (25), (28) and (29) in (24),

$$\| \mathscr{F}[\epsilon]_\omega \|_2 \geq Cf(x'_f) - C\sinh(\| \mathscr{F}[x'_f]_\omega \|_1) \tag{28}$$

Combining (23) and (29),

$$\begin{aligned} Cf(x'_f) - C\sinh(\| \mathscr{F}[x'_f]_\omega \|_1) \\ \leq \| \mathscr{F}[\epsilon]_\omega \|_2 \leq C\sinh(\| \mathscr{F}[x'_f]_\omega \|_1) \end{aligned} \tag{29}$$

We can change the inequality (29) to equality by introducing $p_1, p_2 \in [0, 1]$ such that $p_1 + p_2 = 1$ so that we can form a convex combination [27]. Thus, the inequality (29) becomes,

$$\begin{aligned} f(x'_f) = p_1 \| \mathscr{F}[x'_f]_\omega \|_2 \\ + \frac{p_2}{2}(\sin(\| \mathscr{F}[x'_f]_\omega \|_1 + \sinh(\| \mathscr{F}[x'_f]_\omega \|_1)) \end{aligned} \tag{30}$$

Plugging equation (30) in inequality (29), we get,

$$\begin{aligned} C\{p_1 \| \mathscr{F}[x'_f]_\omega \|_2 + \frac{p_2}{2}\sin(\| \mathscr{F}[x'_f]_\omega \|_1) \\ - \frac{1+p_1}{2}\sinh(\| \mathscr{F}[x'_f]_\omega \|_1)\} \\ \leq \| \mathscr{F}[\epsilon]_\omega \|_2 \leq C\sinh(\| \mathscr{F}[x'_f]_\omega \|_1) \end{aligned} \tag{31}$$

1) By right hand side inequality of (31), $\| \mathscr{F}[\epsilon]_\omega \|_2$ is bounded in one to one correspondence with $\| \mathscr{F}[x'_f]_\omega \|_1$. Therefore, wherever amplitude spectrum of x'_f exists, so would exist amplitude spectrum of ϵ.

Representing $x'_f = \int_0^\infty \mathscr{F}[x'_f]_\omega e^{\iota\omega t} d\omega$, which is the inverse Fourier transform of its Fourier transform,

$$\sin(x'_f) = \sin(\int_0^\infty \mathscr{F}[x'_f]_\omega e^{\iota\omega t} d\omega) \tag{32}$$

Expressing the integral as Riemann sum, we obtain,

$$\sin(x'_f) = \lim_{\delta\omega\to 0} \sin(\sum_i \mathscr{F}[x'_f]_{\omega_i} e^{\iota\omega_i t}\delta\omega) \tag{33}$$

$$\sin(x'_f) = \lim_{\delta\omega\to 0} \sum_{k\geq 0} (-1)^k \frac{(\sum_i \mathscr{F}[x'_f]_{\omega_i} e^{\iota\omega_i t}\delta\omega)^{2k+1}}{(2k+1)!} \tag{34}$$

If $\mathscr{F}[x'_f]_{\omega_i}$ is non-zero at some arbitrary angular frequency ω^*, then separating the corresponding term out of (34),

$$\begin{aligned} \sin(x'_f) \\ = \lim_{\delta\omega\to 0} \sum_{k\geq 0} (-1)^k \\ \times \frac{(\sum_{\omega_i \neq \omega^*} \mathscr{F}[x'_f]_{\omega_i} e^{\iota\omega_i t}\delta\omega + \mathscr{F}[x'_f]_{\omega^*} e^{\iota\omega^* t}\delta\omega)^{2k+1}}{(2k+1)!} \end{aligned} \tag{35}$$

Letting $W = \sum_{\omega_i \neq \omega^*} \mathscr{F}[x'_f]_{\omega_i} e^{\iota\omega t}\delta\omega$, by employing binomial theorem,

$$\begin{aligned} \sin(x'_f) = \lim_{\delta\omega\to 0} \sum_{k\geq 0} \frac{(-1)^k}{(2k+1)!} \\ \times \sum_{n=0}^{2k+1} \binom{2k+1}{n} (W)^{2k+1-n} (\mathscr{F}[x'_f]_{\omega^*} e^{\iota\omega^* t}\delta\omega)^n \end{aligned} \tag{36}$$

$$\begin{aligned} \sin(x'_f) = \lim_{\delta\omega\to 0} \sum_{k\geq 0} \sum_{n=0}^{2k+1} \binom{2k+1}{n} \frac{(-1)^k}{(2k+1)!} \\ \times (W)^{2k+1-n} (\mathscr{F}[x'_f]_{\omega^*}\delta\omega)^n e^{\iota n\omega^* t} \end{aligned} \tag{37}$$

Putting,

$$\begin{aligned} I_{(n,k)}(\omega, \omega^*) = \lim_{\delta\omega\to 0} \binom{2k+1}{n} \frac{(-1)^k}{(2k+1)!} (W)^{2k+1-n} \\ (\mathscr{F}[x'_f]_{\omega^*}\delta\omega)^n \end{aligned} \tag{38}$$

we get,

$$\sin(x'_f) = \sum_{k\geq 0} \sum_{n=0}^{2k+1} I_{(n,k)}(\omega, \omega^*) e^{\iota n\omega^* t} \tag{39}$$

2) It is obvious from equation (39) that sine function extends the spectrum of x'_f to higher frequency domains (but not lower frequency domain), and the support [21] (which is the domain of a function where the function is non-zero) of $\sin(x'_f)$ is not finite.
   It has been ascertained in point (1) that there is one to one correspondence between amplitude spectrum of $\sin(x'_f)$ and x'_f, thus support of x'_f is not finite.
3) Lets define the critical domain as the frequency domain $[-\omega_b, \omega_b]$, such that $|\mathscr{F}[x_o]_\omega|$, and thus $|\mathscr{F}[x'_o]_\omega|$, is non-zero in this domain but zero outside this domain, where ω_b is arbitrary finite angular frequency.
   Suppose spectrum of x_f is zero in critical domain. Then, since $\sin(x'_f)$ distributes the spectrum of x'_f to domain outside the critical domain $[-\omega_b, \omega_b]$, but not in its inside, thus $\mathscr{F}[x'_f]_\omega + C\mathscr{F}[\sin(x'_f)]_\omega$ would be devoid of amplitudes in $[-\omega_b, \omega_b]$, which would lead to the fact that $|\mathscr{F}[x'_o]_\omega|$ or $|\mathscr{F}[x_o]_\omega|$ has no support in $[-\omega_b, \omega_b]$. This would be a contradiction, and thus the domain, where $\mathscr{F}[x_o]_\omega$ has support, $\mathscr{F}[x_f]_\omega$ has support too.

It is a well known fact that $\sin(\phi) < \phi$ for $\phi > 0$. Now let $\phi = |f(x)|$ where $f(x)$ is some arbitrary bounded function having finite support on $x \in \mathbb{R}$, then there would exist following strict inequality by the definition of L_2 norm,

$$\| \sin(f(x)) \|_2 < \| f(x) \|_2 \tag{40}$$

By Plancherel's theorem [21], we can deduce that,

$$\| \mathscr{F}[\sin(f(x))]_\omega \|_2 < \| \mathscr{F}[f(x)]_\omega \|_2 \tag{41}$$

In context of equation (16), above equation can be written as,

$$\| \mathscr{F}[\sin(x'_f(t))]_\omega \|_2 < \| \mathscr{F}[x'_f(t)]_\omega \|_2 \tag{42}$$

4) (42) would imply that $|\mathscr{F}[\sin(x'_f(t))]_\omega|$ covers overall smaller amplitudes, along the whole frequency domain (by Implication B.1.1), as compared to $|\mathscr{F}[(x'_f(t))]_\omega|$.
5) From (16), to achieve x'_o in time domain while only using $\mathscr{F}[x'_f(t)]_\omega$ (as undertaken in TFSP [17]), it is necessary for $\mathscr{F}[\sin(x'_f(t))]$ (scaled by 'C') to cancel out $\mathscr{F}[x'_f(t)]$ outside the critical domain.
It would be impossible for $C\mathscr{F}[\sin(x'_f(t))]$ to completely cancel out $\mathscr{F}[x'_f(t)]$, because then $\| C\mathscr{F}[\sin(x'_f(t))]_\omega \|_2 = \| \mathscr{F}[x'_f(t)]_\omega \|_2$, there would be a contradiction to strict inequality (42).
The failure of this cancellation to happen inside the critical domain is only possible when $\mathscr{F}[x'_f(t)]$ has significantly large amplitudes in that critical domain, as compared to amplitudes outside the frequency domain, and the same constant 'C' would have to increase to be able to cancel out the spectrum inside the critical domain, but then 'C' would not be constant anymore. Thus the amplitude spectrum of $x'_f(t)$, and thus $x_f(t)$ can be identified with large amplitudes inside critical domain, and small amplitudes outside the critical domain.

Hence, point (3) and point (5) prove the principle of SPFS.

REFERENCES

[1] T. Taimre, M. Nikolić, K. Bertling, Y. L. Lim, T. Bosch, and A. D. Rakić, "Laser feedback interferometry: A tutorial on the self-mixing effect for coherent sensing," *Adv. Opt. Photon.*, vol. 7, no. 3, pp. 570–631, 2015.

[2] S. Donati, "Developing self-mixing interferometry for instrumentation and measurements," *Laser Photon. Rev.*, vol. 6, no. 3, pp. 393–417, May 2012.

[3] A. Valavanis *et al.*, "Self-mixing interferometry with terahertz quantum cascade lasers," *IEEE Sensors J.*, vol. 13, no. 1, pp. 37–43, Jan. 2013.

[4] S. Amin, U. Zabit, O. D. Bernal, and T. Hussain, "High resolution laser self-mixing displacement sensor under large variation in optical feedback and speckle," *IEEE Sensors J.*, vol. 20, no. 16, pp. 9140–9147, Aug. 2020.

[5] Y. Zhao, J. Zhou, C. Wang, Y. Chen, and L. Lu, "Temperature measurement of the laser cavity based on multi-longitudinal mode laser self-mixing effect," *IEEE Sensors J.*, vol. 19, no. 12, pp. 4386–4392, Jun. 2019.

[6] P. Dean *et al.*, "Terahertz imaging through self-mixing in a quantum cascade laser," *Opt. Lett.*, vol. 36, no. 13, pp. 2587–2589, 2011.

[7] R. Chhantyal-Pun *et al.*, "Gas spectroscopy with integrated frequency monitoring through self-mixing in a terahertz quantum-cascade laser," *Opt. Lett.*, vol. 43, no. 10, pp. 2225–2228, 2018.

[8] M. Veng, J. Perchoux, and F. Bony, "Fringe disappearance in self-mixing interferometry laser sensors: Model and application to the absolute distance measurement scheme," *IEEE Sensors J.*, vol. 19, no. 14, pp. 5521–5528, Jul. 2019.

[9] G. Giuliani, S. Bozzi-Pietra, and S. Donati, "Self-mixing laser diode vibrometer," *Meas. Sci. Technol.*, vol. 14, no. 1, pp. 24–32, Jan. 2003.

[10] Z. Wei *et al.*, "Obtaining scalable fringe precision in self-mixing interference using an even-power fast algorithm," *IEEE Photon. J.*, vol. 9, no. 4, Jun. 2017, Art. no. 2717947.

[11] Y. Zhang *et al.*, "Broad range and high precision self-mixing interferometer based on spectral analysis with multiple reflections," *IEEE Sensors J.*, vol. 19, no. 3, pp. 926–932, Feb. 2019.

[12] O. D. Bernal, U. Zabit, F. Jayat, and T. Bosch, "Sub-λ/2 displacement sensor with nanometric precision based on optical feedback interferometry used as a non-uniform event-based sampling system," *IEEE Sensors J.*, vol. 20, no. 10, pp. 5195–5203, May 2020.

[13] S. Merlo and S. Donati, "Reconstruction of displacement waveforms with a single-channel laser-diode feedback interferometer," *IEEE J. Quantum Electron.*, vol. 33, no. 4, pp. 527–531, Apr. 1997.

[14] Y. Fan, Y. Yu, J. Xi, and J. F. Chicharo, "Improving the measurement performance for a self-mixing interferometry-based displacement sensing system," *Appl. Opt.*, vol. 50, no. 26, pp. 5064–5072, 2011.

[15] A. Ehtesham, U. Zabit, O. D. Bernal, G. Raja, and T. Bosch, "Analysis and implementation of a direct phase unwrapping method for displacement measurement using self-mixing interferometry," *IEEE Sensors J.*, vol. 17, no. 22, pp. 7425–7432, Nov. 2017.

[16] M. Wang, "Fourier transform method for self-mixing interference signal analysis," *Opt. Laser Technol.*, vol. 33, no. 6, pp. 409–416, Sep. 2001.

[17] U. Zabit, O. D. Bernal, S. Amin, M. F. Qureshi, A. H. Khawaja, and T. Bosch, "Spectral processing of self-mixing interferometric signal phase for improved vibration sensing under weak- and moderate-feedback regime," *IEEE Sensors J.*, vol. 19, no. 23, pp. 11151–11158, Dec. 2019.

[18] H. Wang, Y. Ruan, Y. Yu, Q. Guo, J. Xi, and J. Tong, "A new algorithm for displacement measurement using self-mixing interferometry with modulated injection current," *IEEE Access*, vol. 8, pp. 123253–123261, 2020.

[19] Y. Xiong, H. Chen, X. Wang, T. Feng, H. Yang, and W. Huang, "Improved method for damping coefficient measurement based on spectral analysis of a self-mixing signal," *Appl. Opt.*, vol. 59, no. 8, pp. 2386–2392, 2020.

[20] O. D. Bernal, U. Zabit, and T. Bosch, "Study of laser feedback phase under self-mixing leading to improved phase unwrapping for vibration sensing," *IEEE Sensors J.*, vol. 13, no. 12, pp. 4962–4971, Dec. 2013.

[21] K. Gröchenig, *Foundations of Time-Frequency Analysis*. Boston, MA, USA: Birkhäuser, 2013.

[22] S. L. Brunton and J. N. Kutz, *Data-Driven Science and Engineering: Machine Learning, Dynamical Systems, and Control*. Cambridge, U.K.: Cambridge Univ. Press, 2019.

[23] R. Schafer, "What is a Savitzky-Golay filter? [Lecture notes]," *IEEE Signal Process. Mag.*, vol. 28, no. 4, pp. 111–117, Jul. 2011.

[24] Z. A. Khan, U. Zabit, O. D. Bernal, and T. Hussain, "Adaptive estimation and reduction of noises affecting a self-mixing interferometric laser sensor," *IEEE Sensors J.*, vol. 20, no. 17, pp. 9806–9815, Sep. 2020.

[25] T. Geng, G. Li, Y. Zhang, J. Wang, and T. Zhang, "Phase noise of diode laser in self-mixing interference," *Opt. Exp.*, vol. 13, no. 16, pp. 5904–5912, 2005.

[26] A. A. Siddiqui, U. Zabit, O. D. Bernal, G. Raja, and T. Bosch, "All analog processing of speckle affected self-mixing interferometric signals," *IEEE Sensors J.*, vol. 17, no. 18, pp. 5892–5899, Sep. 2017.

[27] R. T. Rockafellar, *Convex Analysis*, no. 28. Princeton, NJ, USA: Princeton Univ. Press, 1970,